Journal of Computational Physics: X 4 (2019) 100033

Contents lists available at ScienceDirect

Journal of Computational Physics: X

www.elsevier.com/locate/jcpx

On derivatives of smooth functions represented in multiwavelet bases ☆

Joel Anderson [a], Robert J. Harrison [a,*], Hideo Sekino [a], Bryan Sundahl [a], Gregory Beylkin [b], George I. Fann [c], Stig R. Jensen [d], Irina Sagert [e]

[a] Institute for Advanced Computational Science, Stony Brook University, Stony Brook, NY 11794-5250, USA
[b] Department of Applied Mathematics, University of Colorado at Boulder, UCB 526, Boulder, CO 80309-0526, USA
[c] Computer Science and Mathematics Division, Oak Ridge National Laboratory, MS6211, 1 Bethel Valley Road, Oak Ridge, TN 37831-6367, USA
[d] Department of Chemistry, Hylleraas Centre for Quantum Molecular Sciences, UiT The Arctic University of Norway, Mailbox 6050, Langnes N-9037, Tromsø, Norway
[e] Center for Theoretical Astrophysics, Los Alamos National Laboratory, Los Alamos, NM, 87545, USA

ARTICLE INFO

Article history:
Received 12 December 2018
Received in revised form 28 May 2019
Accepted 29 May 2019
Available online 24 July 2019

Keywords:
Multiwavelets
Multiresolution
Derivatives
Numerical
Discontinuous
Bandlimited exponentials

ABSTRACT

We construct high-order derivative operators for smooth functions represented via discontinuous multiwavelet bases. The need for such operators arises in order to avoid artifacts when computing functionals involving high-order derivatives of solutions of integral equations. Previously high-order derivatives had to be formed by repeated application of a first-derivative operator that, while uniquely defined, has a spectral norm that grows quadratically with polynomial order and, hence, greatly amplifies numerical noise (truncation error) in the multiwavelet computation. The new constructions proceed via least-squares projection onto smooth bases and provide substantially improved numerical properties as well as permitting direct construction of high-order derivatives. We employ either b-splines or bandlimited exponentials as the intermediate smooth basis, with the former maintaining the concept of approximation order while the latter preserves the pure imaginary spectrum of the first-derivative operator and provides more direct control over the bandlimit and accuracy of computation. We demonstrate the properties of these new operators via several numerical tests as well as application to a problem in nuclear physics.

1. Introduction

In this paper we revisit the issue of computing high-order derivatives of smooth functions represented in multiwavelet bases. During the development of various flavors of wavelet bases, multiwavelet bases were introduced perhaps as an afterthought. Initially, the whole thrust of wavelet constructions such as Daubechies wavelets [12] or spline wavelets (see e.g. [11]) was to ensure smoothness of a basis. Multiwavelets [1] appeared following a discrete wavelet-like construction in [2] (it turns out that the same bases were sketched earlier in [15] but never used for numerical purposes). While

☆ Anderson, Harrison and Sundahl were supported in part by the NSF under grant ACI-1450344. Jensen was supported by the Norwegian Research Council through the CoE Hylleraas Centre for Quantum Molecular Sciences Grant No. 262695. Sagert was supported in part by DOE grants DE-FG02-87ER40365 and DE-SC0018083. Fann was supported by the Department of Energy under Contract No. DE-AC05-00OR22725.
* Corresponding author.
E-mail address: robert.harrison@stonybrook.edu (R.J. Harrison).

https://doi.org/10.1016/j.jcpx.2019.100033

generalizing the Haar basis [17], multiwavelets kept the "unpleasant" feature that some basis functions are discontinuous. Counter-intuitively, as noted in [3], this feature may be considered "a blessing in disguise". In particular, the fact that the scaling functions are supported on non-overlapping intervals allows high-order schemes on bounded intervals and, also, it is relatively easy to perform nonlinear operations. From an algorithmic point of view, it is also relatively easy to maintain a sparse representation of functions in higher dimensions when compared with required bookkeeping for overlapping bases. The observation that discontinuous basis functions allow high-order schemes is not unique to multiresolution bases as the same has been observed in, e.g., the discontinuous Galerkin methods. Consequently, since representations in multiwavelet bases have many useful properties and result in algorithms well suited for modern computer processors, they became a successful practical tool for high performance computing and are used in quantum chemistry [18,20,45,46] and nuclear physics [34,14,31,32], and serve as mathematical underpinnings of MADNESS [21].

Yet, the fact that basis functions are allowed to be discontinuous leads to a number of problems. As discussed in [3], the only scale-consistent derivative operator available to us is the first derivative. Operators for the second and higher derivatives do not exist due to the discontinuous nature of the basis and are applied as a power of the first derivative. Naively, if the function has high-order derivatives, such an approach appears reasonable. However, due to the approximate nature of representation in multiwavelet bases there are ϵ-size discontinuities between representations on neighboring intervals (where ϵ is user-selected) and repeated applications of derivative operators may lead to large errors and the appearance of spiky artifacts at boundaries of intervals. While in many instances differential equations can be replaced by integral equations as in [18,20,45,46], the evaluation of high order derivatives of solutions is a necessary step in computing functionals that carry physical meaning. An interesting observation was made in [13]: while the basis functions are not smooth, given multiwavelet coefficients one can look for a function with the maximal number of derivatives that has these coefficients. In that approach, coefficients remain unchanged and the function interpreted as having derivatives in bases dual to multiwavelets.

The main ideas of our approach are as follows.

1. We assume that the input coefficients are (slightly) corrupted and, for this reason, first project the function onto a smooth basis and then use this projection to differentiate the original function. If we were to take the projection and compute its multiwavelet coefficients, they will slightly differ from the original ones. This approach permits the construction of first, second, and higher derivatives.
2. Two smooth intermediate bases are explored. While we can safely assume that splines are well known, we introduce exponential bases for bandlimited functions in greater detail since such bases are less known. We use them as an alternative to projections on splines to emphasize the generic nature of our approach and, also, due to remarkable properties of the resulting operators.
3. The construction for all bases retains the 3-box stencil of the original derivative operator and for b-splines also retains the same order of approximation, and hence the new operators can be used as a drop-in replacement in the software. For bandlimited exponentials, the concept of order of approximation is maintained to the accuracy of the underlying quadrature and the associated bandlimit.

Our numerical results for up to third-order derivatives demonstrate that the new operators display the expected order of approximation and are substantially superior in controlling both pointwise and normwise errors in derivatives, especially with noisy input functions. Also demonstrated is improved consistency between the derivative operators and their pseudo-inverse (i.e., convolution with the corresponding Green's function). We will see that the original operator retains some advantages, notably in computing the quantum mechanical kinetic energy to high accuracy.

Motivating our work are applications in the structure of nuclear matter [34,14,31,32] and molecular electronic structure [43,47,45,46,48,9,16,20] composed within the MADNESS framework [21] and the independent MRChem package [25]. Both disciplines employ the Kohn-Sham formulation of density functional theory (DFT) [30] that expresses the energy as a functional of the density that is in turn parameterized by a set of orthonormal one-particle orbitals (i.e., one-particle wave functions). Variation of the orbitals to minimize the energy while enforcing the orthonormality constraint yields a non-linear eigenvalue problem (a set of coupled differential equations) that for accurate and efficient computation within the multiwavelet basis is recast into a set of coupled integral equations. In the molecular problem the orbitals can usually be chosen as real-valued functions of the position of an electron in 3D space, and the occupied (i.e., bound or negative energy) orbitals will asymptotically decay exponentially to satisfy free-space boundary conditions. In the nuclear problem the orbitals will typically be 2-component spinors with each component being a complex-valued function of the position of a nucleon, and both occupied and unoccupied (unbound or positive energy) states must be computed for energy functionals that incorporate superfluidity. The unbound states are not exponentially localized and other techniques are necessary to map the computation onto a finite volume [32]. While the DFT energy functionals are quite different for nuclei and electrons, they have multiple elements in common including the incorporation of first, second and higher derivatives of the electron density as well as strongly non-linear functions of these. Properties beyond those of the ground state (e.g., excitation energies or the response to external perturbations such as time-dependent electric or magnetic fields) require even higher derivatives. The amplification of numerical noise inherent in computing higher derivatives with the original scheme, the sensitivity of some non-linear functionals to point-wise rather than norm-wise errors, and the sensitivity of some functionals to regions where the density is small (and hence potentially dominated by numerical noise), combine to

make computations with functionals that incorporate derivatives more expensive compared to those that do not include derivatives. This is largely due to the need to compute much more accurately (i.e., oversample) in order to obtain accurate derivatives and function tails.

Another issue arising from the norm of the original derivative operator and the need to compute higher derivatives by its repeated application is that differential operators and their pseudo-inverse (i.e., convolution with the corresponding Green's function) do not numerically commute within the precision of computation — i.e., the order of operations matters and there is a lack of consistency between the numerical and formal calculus. This has emerged as a significant issue for scientists making first use of MADNESS, which typically requires reformulating partial differential equations as integral equations with free-space or periodic boundary conditions. Nominally equivalent expressions may have very different error properties that can affect both accuracy and convergence. For instance, in the electronic structure problem it is appealing to compute a residual from the standard eigenvalue problem in differential form while updating the orbitals using the Green's function to the bound-state Helmholtz (BSH) equation (which builds in desirable physics in addition to being numerically efficient; [19]). However, this fails to converge robustly to high accuracy since the available Laplacian operator strongly amplifies high frequency noise that is suppressed by the integral operator. In the results section we will see that the new differential operators significantly improve upon prior behavior.

We note that there is a large number of publications on constructing derivative operators (in the form of a finite difference scheme) with additional desired properties - for example TVD [22,36,23] or WENO [24,29]. However, in this case the difficulty addressed is how to differentiate accurately and avoid artifacts in a scheme where a function develops a shock, a rapid variation over a small interval. Note that we are addressing an "opposite" problem where functions are known to be differentiable many times but are represented via functions that have discontinuities. In molecular electronic structure the solutions are smooth except for cusps at the known locations of the nuclear centers if point nuclear charges are used, however it is routine to eliminate these cusps either analytically or through the use of effective potentials. Another issue in constructing derivative operators addressed in [7,35,26] is how to avoid spurious eigenvalues of such operators (that necessarily occur when using polynomial bases), which negatively affect the operator norm. We obtain a similar result in our construction when using bandlimited exponentials.

This returns us to the basic concept of this paper — the multiwavelet basis is very convenient for efficiently computing with locally-refined representations of functions and operators, and we can circumvent some of the deficiencies of the multiwavelet basis by constructing operator representations in an underlying basis selected to provide the desired properties. We briefly introduce the multiwavelet basis, review the construction and form of the original derivative operator, and then introduce our new constructions. Subsequently, we present and discuss numerical results and conclusions.

2. The multiwavelet basis

The multiwavelet scaling functions [1] are given by scaled and normalized Legendre polynomials defined on $[0, 1]$,

$$\phi_i(x) = \begin{cases} \sqrt{2i+1}P_i(2x-1), & x \in [0,1] \\ 0, & x \notin (0,1) \end{cases}, \tag{1}$$

where $i = 0, \ldots, k-1$, k is the order of the basis (i.e., the first k polynomials are used), $P_i(x)$ are the Legendre polynomials, and $\sqrt{2i+1}$ is a normalization factor. From these the scaling functions in the l^{th} box at level n are formed by translation and dilation

$$\phi_{il}^n(x) = 2^{n/2}\phi_i(2^n x - l) \tag{2}$$

By construction these functions form an orthonormal basis at level n.

Alpert's construction [1] of the wavelet basis starts with the two-scale relationship between polynomials at level n and $n-1$

$$\phi_i^{n-1}(x) = \sqrt{2}\sum_{j=0}^{k-1}(h_{ij}^{(0)}\phi_j^n(2x) + h_{ij}^{(1)}\phi_j^n(2x-1)), \quad i = 0, \ldots, k-1, \tag{3}$$

where $H^{(0)} = \left\{h_{ij}^{(0)}\right\}$ and $H^{(1)} = \left\{h_{ij}^{(1)}\right\}$ are the filter coefficients, which are readily computed by orthogonal projection. The orthonormal wavelets at level $n-1$ are similarly expanded in terms of the scaling functions at level n

$$\psi_i^{n-1}(x) = \sqrt{2}\sum_{j=0}^{k-1}(g_{ij}^{(0)}\phi_j^n(2x) + g_{ij}^{(1)}\phi_j^n(2x-1)), \quad i = 0, \ldots, k-1, \tag{4}$$

where the filter coefficients $G^{(0)} = \left\{g_{ij}^{(0)}\right\}$ and $G^{(1)} = \left\{g_{ij}^{(1)}\right\}$ are again computed by orthogonal projection noting that the wavelets are orthogonal to the scaling functions at the same and coarser levels, and that the wavelets are orthogonal to each

other across all scales. Together, these relations enable the transformation between different scales of the multiresolution analysis. Note that at their mid-point the multiwavelets (4) are either discontinuous or have a discontinuous derivative.

The projection of a function $f(x)$ into the order-k scaling function basis at level n is

$$f^n(x) = \sum_{l=0}^{2^n-1} \sum_{j=0}^{k-1} s_{jl}^n \phi_{jl}^n(x), \tag{5}$$

where s are the scaling function coefficients. Assuming f is k-times differentiable, the approximation error is [1]

$$\left\| f - f^n \right\| \leq 2^{-nk} \frac{2}{4^k k!} \sup_{x\in[0,1]} \left| \frac{d^k}{dx^k} f(x) \right|. \tag{6}$$

Repeated application of the filters $H^{(0)}$, $H^{(1)}$, $G^{(0)}$ and $G^{(1)}$ (i.e., the fast wavelet transform [4]) performs the orthogonal transformation into the corresponding wavelet representation

$$f^n(x) = \sum_{j=0}^{k-1} \left(s_{j0}^0 \phi_j(x) + \sum_{m=0}^{n-1} \sum_{l=0}^{2^m-1} d_{jl}^m \psi_{jl}^m(x) \right).$$

Adaptive refinement is accomplished by discarding small wavelet coefficients according to user-specified criteria. The wavelet coefficients will be small below the refinement level at which the function locally becomes well approximated by the Legendre basis. Thus, the noise or error in numerical computation has a known form — it is dominated, for smooth functions, by wavelets at the next finest scale.

2.1. Derivative operator

As discussed in the introduction, there is just one scale-consistent derivative operator in this basis, which may be obtained either by seeking the unique operator that is homogeneous of degree one, or by projection and integration by parts as is traditionally done to obtain the weak derivative [3]. Free parameters in the operator permit incorporation of boundary conditions and construction of forward, central, or backward forms. In this paper we just consider the central (or periodic) form.

Given the projection (5) of a function at level n, the scaling function coefficients ($\bar{s}_{lj}^n$) of the derivative in box l at level n are related to the input coefficients from the corresponding box and its neighbors ($l-1$ and $l+1$) by the transition matrices r_{-1}, r_0, and r_1 of a 3-block stencil

$$\bar{s}_{jl}^n = \sum_{i=0}^{k-1} [r_1]_{ji}\, s_{il-1}^n + [r_0]_{ji}\, s_{il}^n + [r_{-1}]_{ji}\, s_{il+1}^n, \tag{7}$$

with $r_{-1} = -r_1^t$. For this unique, scale-consistent derivative operator, we also have that the central block is skew-symmetric, i.e., $r_0 = -r_0^t$ so that the entire operator is skew-symmetric. This property will not hold for the smoothed derivatives constructed below.

3. Construction of smoothing differential operators

The scale-consistent construction of the derivative operator [3] proceeds with the perspective that the function being differentiated is the expansion in the discontinuous scaling function (or equivalently multiwavelet) basis. Here, we instead change this perspective and assume that the expansion in scaling functions is an approximation to some at least p-differentiable function about which we know only approximations to the first few generalized moments within each box — i.e., the expansion coefficients are interpreted as the projection of this smooth function into the local Legendre polynomial basis of order k, with these coefficients only being known to the precision of computation. We construct local representations of this smooth function by projecting into a smooth basis that is at least p-differentiable and which is defined over the domain of the derivative operator (a 3-box stencil). The projection is performed in a least-squares sense so as to reproduce as accurately as possible the known moments (i.e., expansion coefficients with respect to scaling functions). With this smooth representation in hand, the derivative is computed and expansion in the scaling function basis recovered by orthogonal projection. In practice all three operations (projection into the smooth basis, differentiation, projection into the scaling function basis) are combined into a single matrix representation.

By applying the smoothing locally at the same scale at which the scaling function expansion is known, we accommodate adaptive refinement (that can introduce noise at any scale) and do not enforce a global band limit that would limit applicability. Together with increasing the accuracy/band-limit/order of the smooth basis in tandem with that of the scaling function basis, we preserve the ability to control the overall accuracy of computation through either adaptive refinement or use of a higher-order basis (larger k). Therefore, no new parameters are introduced that control the error in computation.

The construction preserves the 3-box stencil and scale-invariant operator, and hence can be used as a drop-in replacement in existing software (e.g., MADNESS [21], MRChem [25]).

We now explain our construction in a general setting that combines the projection and differentiation operators. Let us assume that we have two bases, the original basis $u_1(x), u_2(x), \dots u_n(x)$ and an auxiliary basis $v_1(x), v_2(x), \dots v_m(x)$, where $m \le n$ and the latter basis spans a subspace of the former (exactly or approximately within a given accuracy). Specifically, we are interested in the case where the basis functions $v_1, v_2, \dots v_m$ all have derivatives of order p whereas not all of the functions $u_1(x), u_2(x), \dots u_n(x)$ are p-differentiable. As we already pointed out, our main example is the basis where $u_1(x), u_2(x), \dots u_n(x)$ are piece-wise polynomials.

We assume that the function f has the derivative of order p that we want to evaluate but is written in the original basis,

$$f(x) = \sum_{k=1}^{n} f_k u_k(x) + O(\varepsilon), \tag{8}$$

where ε is the accuracy of computation. Note that if the coefficients f_k are known exactly then the error would be entirely in the wavelet spaces at the current and finer scales, but in practice the coefficients would only be known approximately.

Let us start by defining the $n \times m$ matrix $\mathbf{A}$ with entries

$$\alpha_{il} = \int u_i(x) v_l(x) dx, \tag{9}$$

and, if the original basis is not orthonormal, also the $n \times n$ Gram matrix $\mathbf{G}$ with entries

$$G_{ik} = \int u_i(x) u_k(x) dx, \;\; i,k = 1, \dots n.$$

Our first step is to project f on the subspace spanned by functions $v_1(x), v_2(x), \dots v_m(x)$ reproducing in a least squares sense the projection onto the original basis. We seek the coefficients g_l so that

$$\sum_{k=1}^{n} f_k u_k(x) \approx \sum_{l=1}^{m} g_l v_l(x). \tag{10}$$

Denoting $\mathbf{f} = (f_1, f_2, \dots f_n)$, $\mathbf{g} = (g_1, g_2, \dots g_m)$ and projecting from the left with $u_i(x)$, we seek $\mathbf{g}$ such that

$$\mathbf{A}^*\mathbf{G}\mathbf{f} = \mathbf{A}^*\mathbf{A}\mathbf{g}.$$

Thus, we obtain coefficients of f in the auxiliary basis as

$$\mathbf{g} = \left(\mathbf{A}^*\mathbf{A}\right)^{-1} \mathbf{A}^*\mathbf{G}\mathbf{f}$$

and write

$$f(x) = \sum_{l=1}^{m} g_l v_l(x).$$

Next, we apply the derivative of order p to the function f and obtain

$$\frac{d^p}{dx^p} f(x) = \sum_{l=1}^{m} g_l \frac{d^p}{dx^p} v_l(x).$$

In order to return to a representation in the original basis, we project the derivative $\frac{d^p}{dx^p} v_l(x)$ on functions u_i,

$$\beta_{il}^{(p)} = \int u_i(x) \frac{d^p}{dx^p} v_l(x) dx, \;\; i = 1, 2, \dots, n, \;\; l = 1, 2, \dots m.$$

Denoting by $\mathbf{B}^{(p)}$ the $n \times m$ matrix with entries $\beta_{il}^{(p)}$, we obtain the coefficients of the pth derivative of function f in the original basis as

$$\mathbf{f}^{(p)} = \mathbf{G}^{-1}\mathbf{B}^{(p)}\mathbf{g}$$

or

$$\mathbf{f}^{(p)} = \mathbf{G}^{-1}\mathbf{B}^{(p)} \left(\mathbf{A}^*\mathbf{A}\right)^{-1} \mathbf{A}^*\mathbf{G}\mathbf{f}$$

and define the differentiation matrix as

$$\mathbf{D}^{(p)} = \mathbf{G}^{-1}\mathbf{B}^{(p)}\left(\mathbf{A}^*\mathbf{A}\right)^{-1}\mathbf{A}^*\mathbf{G}.$$

If the original basis $u_1, u_2, \ldots u_n$ is orthonormal, then $\mathbf{G}$ is the identity matrix and we have

$$\mathbf{D}^{(p)} = \mathbf{B}^{(p)}\left(\mathbf{A}^*\mathbf{A}\right)^{-1}\mathbf{A}^*. \tag{11}$$

In our case the first basis consists of the multiwavelet scaling functions (a.k.a. the normalized Legendre polynomials or, alternatively, the normalized Lagrange interpolating polynomials) in the three adjacent intervals and the second basis is either that of splines or of band-limited functions on the combined three-box intervals.

3.1. Derivative operators using B-splines

As an auxiliary basis, a b-spline basis functions of order M are formed from piecewise polynomials of degree $M-1$ and spans $M+1$ knots. Derivatives up to order $M-2$ are continuous across the domain. We employ N knots uniformly distributed over $[-1,2]$ (i.e., the union of the three boxes $[-1,0]$, $[0,1]$ and $[1,2]$), with the location of the ith knot $(i=0,\ldots,N-1)$ given by $x_i = \frac{3i}{N-1} - 1$. Using these knots we construct the full spline basis of order M, repeating knots as necessary at the end points. Associated with each end point there are $M-1$ splines with repeated knots, and in the interior there are $N-M$ splines without repeated knots. Thus, there is a total of $N+M-2$ functions in the basis. The b-splines with support including the center region $[0,1]$ correspond to the cardinal splines, which have Fourier transform proportional to $(\mathrm{sinc}(\omega))^{M-1}$. It is this property that provides the primary source of smoothing.

Choosing the b-spline basis to have the minimum order necessary such that the pth derivative results in splines of order k, we identify $M = k+p$. This choice is consistent with projection of the derivative back into the Legendre polynomial basis of order k, and is also the minimum order necessary to obtain non-zero approximations to the first or second derivatives when computing with the Haar (piecewise constant) basis. Furthermore, Theorem 2 of [42] establishes that, with this choice of M, there exists a b-spline approximation to an appropriately smooth function $f(x)$ such that the error in the pth derivative of the approximation is $O\left(c(k,p)2^{-nk}\right)$, where n is the level of refinement in the dyadically-refined adaptive mesh so the box size at level n is $O\left(2^{-n}\right)$, and $c(k,p)$ is some constant independent of n. This error, which is numerically verified in the results section, is of the same order as that of the projection of a smooth function into the order-k Legendre basis (6) and with that of the original derivative operator [3]. Remarkably, the pth derivative ($p \le 2k$) is exact if the input function $f(x)$ is exactly a polynomial of degree $k+p-1$ or less over the entire domain $[-1,2]$ despite the intermediate projection into the discontinuous scaling function basis that includes only polynomials up to degree $k-1$ within each of the sub-intervals $[-1,0]$, $[0,1]$ and $[1,2]$. This is due to the linear least-squares reproduction of the moments (expansion coefficients in the scaling function basis) having the exact expansion of the polynomial in the b-spline basis as its unique, zero-residual solution.

In this work we chose the number of knots $N = k+1$ independent of p. The primary motivations for this are that it is again the minimum number necessary to construct first and second derivatives for the Haar basis, and for the first derivative ($p=1$) this choice yields $2k$ degrees of freedom in the spline basis to be compared with $3k$ degrees of freedom in the input basis (i.e., the first k Legendre polynomials in each of the 3 boxes). Thus, there is additional smoothing resulting from the fitting to the lower dimension basis, which was thought to be desirable from the perspective of suppressing noise. Other choices are clearly feasible, however, this choice has proved satisfactory and limited experimentation did not identify any clearly superior choices.

3.2. Derivative operators using bandlimited exponentials

Instead of using b-splines as an auxiliary basis in the construction of smoothing derivative operators, we can use bandlimited exponentials (which are not necessarily periodic on an interval). The reasons to use these functions instead of piece-wise polynomials are: first, it further clarifies our approach to constructing "non-native" derivative operators in multiwavelet bases and, second, the resulting operators have remarkable properties which we describe below. As a practical matter, the accuracy of the results obtained using such derivatives is similar to those obtained using b-splines.

Polynomial approximations have a long tradition in numerical analysis and lead, *inter alia,* to the notion of the order of convergence of numerical schemes. For smooth periodic functions a well known alternative is to use approximations via trigonometric polynomials (i.e., via a truncated Fourier series). For bandlimited non-periodic functions on an interval a natural basis is that of eigenfunctions of the band-and-time limiting operator introduced in a series of seminal papers by Slepian, Landau and Pollak, [41,27,28,37–40], where they observed that the eigenfunctions of such operator are the Prolate Spheroidal Wave Functions (PSWFs) of classical Mathematical Physics. Instead of using PSWFs directly (which is a possible choice), we use bandlimited exponentials constructed in [5,6] to provide us an approximate auxiliary basis.

We observe that while smooth periodic band-limited functions may be represented via a truncated Fourier series, the Fourier series is not efficient for band-limited but non-periodic functions on an interval. This motivates considering a linear space of functions admitting a representation via exponentials $\left\{e^{ibx}\right\}_{|b|\le c}$, $x \in [-1,1]$,

$$\mathcal{E}_c = \left\{ u \in L^\infty([-1,1]) \;\middle|\; u(x) = \sum_{k\in\mathbb{Z}} a_k e^{icb_k x} : \{a_k\}_{k\in\mathbb{Z}} \in l^1,\ b_k \in [-1,1] \right\},$$

where c (bandlimit) is a fixed parameter (see [5,6]). We seek (an approximate) basis for this space. While PSWFs can serve this purpose, it is more convenient in our case to use a fixed set of exponentials $\left\{e^{ic\theta_k x}\right\}_{k=1}^{M}$ as described in the sequel.

The use of band-limited functions on an interval for integration and interpolation relies on quadratures constructed in [44,5,33].[1] These Gaussian-type quadratures for bandlimited exponentials differ from the classical Gaussian quadratures for polynomials in that they are approximate. Indeed, with a finite number of nodes it is impossible to integrate exactly an infinite number of functions but, it turns out, that all functions $\mathcal{E}_c$ can be integrated within any finite user-selected accuracy ϵ. The generalized Gaussian quadratures for exponentials to integrate functions in $\mathcal{E}_c$ with accuracy ϵ are summarized as (see [5,33,6])

Lemma. *For $c > 0$ and any $\epsilon > 0$, there exist a finite number of nodes $-1 < \theta_1 < \theta_2 < \cdots < \theta_M < 1$ and corresponding weights $w_k > 0$, such that for any $x \in [-1, 1]$,*

$$\left| \int_{-1}^{1} e^{ictx}\, dt - \sum_{k=1}^{M} w_k e^{ic\theta_k x} \right| < \epsilon, \tag{12}$$

where the number of nodes, $M = c/\pi + O(\log c)$, is (nearly) optimal. The nodes and weights maintain the natural symmetry, $\theta_k = -\theta_{M-k+1}$ and $w_k = w_{M-k+1}$.

We note that the construction of quadratures in [5,33] is more general than formulated here and yields quadratures for band-limited exponentials integrated with a weight function.

We now describe interpolation in $\mathcal{E}_c$. Given a finite accuracy ϵ, we seek to represent functions in $\mathcal{E}_c$ by a fixed set of exponentials $\left\{e^{ic\theta_k x}\right\}_{k=1}^{M}$, where M is as small as possible. It turns out (see [5]) that by finding quadrature nodes $\{\theta_k\}_{k=1}^{M}$ and weights $\{w_k\}_{k=1}^{M}$ for exponentials with bandlimit $2c$ and accuracy ϵ^2, we in fact obtain an approximate basis to represent all exponentials in $\mathcal{E}_c$ with accuracy ϵ. As a basis, the set of exponentials $\left\{e^{ic\theta_k x}\right\}_{k=1}^{M}$ is similar to monomials (as well as to exponentials in the Fourier series), whereas the PSWFs are strikingly similar to orthogonal polynomials. While, as a general rule, it is preferable to work with orthogonal bases, since we use only the final result in constructing derivative operators, we work directly with the basis $\left\{e^{ic\theta_k x}\right\}_{k=1}^{M}$ and use extended precision to address ill-conditioning. Once the necessary matrices are computed one can use them in computations with the standard double precision. When building derivative operators using exponentials, it is more convenient to first split the interval $[-1, 1]$ into three subintervals, construct the operators on these subintervals, and then rescale the result to intervals $[-1, 0]$, $[0, 1]$ and $[1, 2]$ that have been used for b-splines.

Our first step is to expand the functions $\left\{e^{ic\theta_k x}\right\}_{k=1}^{M}$ on $[-1, 1]$ into the basis of the Legendre polynomials on intervals $[-1, -1/3]$, $[-1/3, 1/3]$ and $[1/3, 1]$. We denote the orthonormal scaling functions of a multiwavelet basis (i.e. normalized Legendre polynomials) on intervals $[-1, -1/3]$, $[-1/3, 1/3]$ and $[1/3, 1]$ as $\left\{\phi_i^-(x)\right\}_{i=0}^{i=k-1}$, $\left\{\phi_i^c(x)\right\}_{i=0}^{i=k-1}$ and $\left\{\phi_i^+(x)\right\}_{i=0}^{i=k-1}$, and compute coefficients

$$A_{im}^- = \int_{-1}^{-1/3} e^{ic\theta_m x} \phi_i^-(x)\, dx$$

$$A_{im}^c = \int_{-1/3}^{1/3} e^{ic\theta_m x} \phi_i^c(x)\, dx,$$

and

$$A_{im}^+ = \int_{1/3}^{1} e^{ic\theta_m x} \phi_i^+(x)\, dx,$$

where $i = 0, \ldots k-1$ and $m = 1, \ldots, M$. Following (9), we then merge these three matrices to form $3k \times M$ matrix $\mathbf{A} = \{A_{im}\}_{\substack{i=1,\ldots,3k \\ m=1,\ldots,M}}$, where $3k \geq M$. We choose the relation between the number of nodes M and the order of the basis k so that the basis functions $\left\{e^{ic\theta_k x}\right\}_{k=1}^{M}$ are approximated by the Legendre polynomials of degrees up to $k-1$ on the sub-intervals

[1] These quadratures allow us to break with the conventional approach of using polynomials and lead to improvements in performance of algorithms for interpolation, estimation and solving partial differential equations (see e.g. [7,35,26,8]). The improvements have to do with being able to approach the Nyquist rate for bandlimited functions on the real line while working with bandlimited functions on an interval.

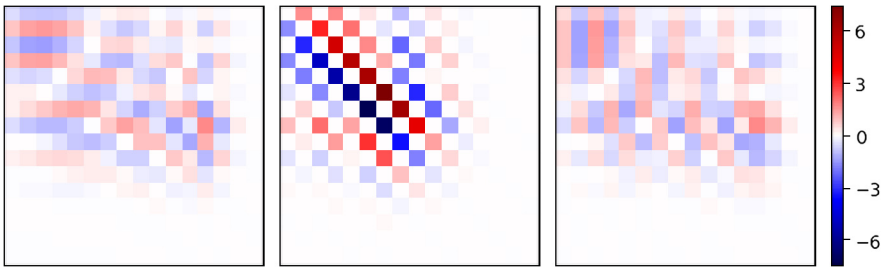

Fig. 1. Density plot of three blocks of the derivative matrix for $k = 16$ with a resulting accuracy of approximately 10^{-7}.

$[-1, -1/3]$, $[-1/3, 1/3]$ and $[1/3, 1]$ with accuracy ϵ, where ϵ is the accuracy of representing exponentials in $\mathcal{E}_c$ via the basis functions.

Given a bandlimited (or approximately bandlimited) function in $\mathcal{E}_c$,

$$f(x) = \sum_{m=1}^{M} g_m e^{ic\theta_m x}, \tag{13}$$

we denote the vector of its coefficients as $\mathbf{g} = \{g_m\}_{m=1}^{M}$. Using matrix $\mathbf{A}$, we obtain the coefficients of this function in the Legendre basis on the union of three subintervals as

$$\mathbf{f} = \mathbf{A}\mathbf{g}. \tag{14}$$

Next we compute the derivative of f in (13) as

$$f'(x) = ic \sum_{m=1}^{M} g_m \theta_m e^{ic\theta_m x},$$

noting that the generalization to higher order derivatives is straightforward. Denoting by $\mathbf{S}$ the diagonal matrix,

$$\mathbf{S} = ic\,\mathrm{diag}\,(\theta_1, \theta_2, \ldots \theta_M)\,, \tag{15}$$

we compute coefficients of the derivative in the Legendre basis as

$$\mathbf{f}' = \mathbf{A}\mathbf{S}\mathbf{g}.$$

Since we want to map $\mathbf{f}$ directly into $\mathbf{f}'$, we estimate $\mathbf{g}$ from (14) by using the normal equation $\mathbf{A}^*\mathbf{A}\mathbf{g} = \mathbf{A}^*\mathbf{f}$,

$$\mathbf{f}' = \mathbf{A}\mathbf{S}\left(\mathbf{A}^*\mathbf{A}\right)^{-1}\mathbf{A}^*\mathbf{A}\mathbf{g} = \mathbf{A}\mathbf{S}\left(\mathbf{A}^*\mathbf{A}\right)^{-1}\mathbf{A}^*\mathbf{f}.$$

The $3k \times 3k$ derivative matrix is then

$$\mathbf{D} = \mathbf{A}\mathbf{S}\left(\mathbf{A}^*\mathbf{A}\right)^{-1}\mathbf{A}^*, \tag{16}$$

where $(\mathbf{A}^*\mathbf{A})^{-1}\mathbf{A}^*$ is the pseudo-inverse of $\mathbf{A}$. All computations must be done with the extended precision to account for ill-conditioning of $\mathbf{A}$ but, once computed, the resulting matrix $\mathbf{D}$ can be used in the standard precision.

Remarkably, while the resulting matrix $\mathbf{D}$ is not anti-symmetric, its eigenvalues are either pure imaginary or zeros. Indeed, on its range matrix $\mathbf{D}$ is similar to $\mathbf{S}$ as it follows from (16). Extracting three middle blocks of the matrix $\mathbf{D}$, each of them of size $k \times k$, re-scaling them by the factor $\frac{2}{3}$, we obtain the derivative operator with smoothing by projection on bandlimited functions with the bandlimit $\frac{2}{3}c$. The factor $\frac{2}{3}$ accounts for switching from the interval $[-1, 1]$ (of length 2) to the interval $[-1, 2]$ (of length 3) which we used in constructing spline-based projections.

The sub-matrices comprising the resulting derivative operator are illustrated in Fig. 1. There is no observed symmetry between or within the blocks and the off-diagonal blocks are not rank one as in the case of the multiwavelet derivative.

Similarly, the second derivative is constructed as

$$\mathbf{D}^2 = \mathbf{A}\mathbf{S}\left(\mathbf{A}^*\mathbf{A}\right)^{-1}\mathbf{A}^*\mathbf{A}\mathbf{S}\left(\mathbf{A}^*\mathbf{A}\right)^{-1}\mathbf{A}^* = \mathbf{A}\mathbf{S}^2\left(\mathbf{A}^*\mathbf{A}\right)^{-1}\mathbf{A}^*$$

and we use its three middle blocks. Again, we observe that the resulting $3k \times 3k$ matrix $\mathbf{D}^2$ is not symmetric but has only negative or zero eigenvalues. Higher order derivatives are obtained in a similar manner (note that in (11) $\mathbf{B}^{(p)} = \mathbf{A}\mathbf{S}^p$).

Since on its range matrix $\mathbf{D}$ is similar to $\mathbf{S}$, the norm of the derivative operator $\mathbf{D}^p$ is controlled by the norm of $\mathbf{S}^p$ which does not exceed c^p, where c is the bandlimit (15). As in [7,35,26], we thus avoid spurious eigenvalues that necessarily occur

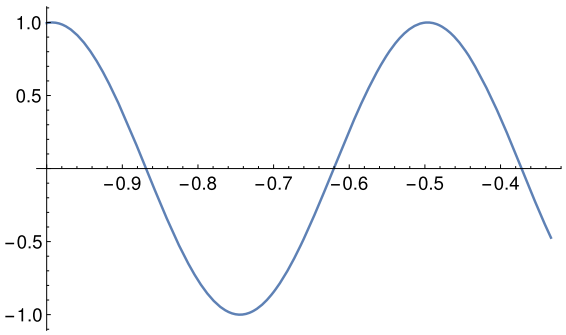

Fig. 2. An example of a basis function, $e^{ic\theta_5 x}$, from the set $\left\{e^{ic\theta_k x}\right\}_{k=1}^{M}$, where $M = 25$ displayed on the interval $[-1, -1/3]$. Such functions are approximated by a linear combination of the Legendre polynomials of degrees $i = 0, \ldots k-1$, where in 1 we used $k = 16$ (yielding accuracy $\approx 3 \cdot 10^{-7}$).

when using polynomial bases. The choice of the bandlimit c depends on the order of the multiwavelet basis which in turn depends on the problem being solved and the desired accuracy.

As an example, we use basis $\left\{e^{ic\theta_k x}\right\}_{k=1}^{M}$, where $M = 25$, and the bandlimit $c = 15.70796326794900$ and display one of the functions, $e^{ic\theta_5 x}$, on the interval $[-1, -1/3]$ in Fig. 2. As scaling functions, we use the Legendre polynomials of degrees $i = 0, \ldots k-1$, where $k = 16$, approximating the basis $\left\{e^{ic\theta_k x}\right\}_{k=1}^{M}$ separately on the sub-intervals $[-1, -1/3]$, $[-1/3, 1/3]$ and $[1/3, 1]$ with accuracy $\epsilon \approx 3 \cdot 10^{-7}$. As described above, we create a $3k \times 3k$ derivative matrix and then extract three $k \times k$ blocks to be used as the first derivative operator. These three 16×16 matrices are displayed in Fig. 1.

4. Demonstration and discussion

4.1. Point-wise errors

In Fig. 3, we examine the nature of local errors in the derivatives by repeated application of the first derivative operator to a 3D Gaussian and plotting along the x-axis the absolute error from the exact results. By varying the level at which the Gaussian is projected into the scaling function basis we explore from low accuracy and under sampling (level $n = 4$) to high accuracy and over sampling ($n = 7$). It is apparent how the original derivative operator amplifies the discontinuities at the edges of the sampling boxes (the computation is in the cube $[-16, 16]^3$ so the boxes at level n have size 2^{5-n}), with repeated application to obtain higher derivatives magnifying this effect. Refinement also magnifies this defect in the original operator with an extra factor of about 2 with each level of refinement. To explain the main origin of this effect, consider the function $(1 + \mathrm{erf}(2^n x))\epsilon/2$ which is a smooth approximation to a step discontinuity of height ϵ at scale n — its derivative at $x = 0$ is $2^n/\pi$. The maximum value of the derivative necessarily increases at finer scales in order to preserve the magnitude of its integral. The other two constructions greatly suppress the impact of these artifacts of the discontinuous basis. At low refinement ($n = 4$), the original first-derivative operator performs slightly better than the b-spline and BLE operators — presumably their filtering is discarding essential information in the high-frequencies, and since the BLE operator filters most strongly (see Fig. 9) it performs the least well. With increasing accuracy/refinement ($n = 5, 6, 7$), the original operator performs increasingly worse relative to the b-spline operator that is able to attain high precision. At intermediate refinement ($n = 5$), the b-spline and BLE operators behave similarly. However, at deeper refinement ($n = 6, 7$), the accuracy of the quadrature used in the construction of the BLE operator dominates the error (in this case around 10^{-9}) since accuracy of computation is higher than that of the quadrature. While it is possible to construct a higher accuracy quadrature, it is not typical that we compute to greater than 10 significant digits.

In Fig. 4, using the same test 3D test function, for the b-spline and BLE constructions we contrast the size of local errors obtained by repeated application of the first derivative operator ($\left(\frac{d}{dx}\right)^p$ for $p = 2, 3$) with those from direct application of the high-order derivative operator ($\frac{d^p}{dx^p}$) constructed as described in Section 3. For the second derivative, repeated versus direct application have fairly comparable errors. However, for the third derivative (available for the b-spline only) it is apparent that repeated application at deeper refinement (or higher accuracy) has a significant advantage over the direct application. Both rules should have the same order accuracy (by construction in Section 3.1 and numerically demonstrated in Figs. 6 and 7), and we instead attribute this to the repeated application corresponding to a 7-box stencil and rather than just the 3-box stencil of the direct application.

4.2. Norm-wise properties and errors

The spectral norm of the three operators (largest singular value of the rectangular matrix representation) was computed as a function of k (Fig. 5). As expected, the norm of the original operator grows quadratically with k, whereas the other two

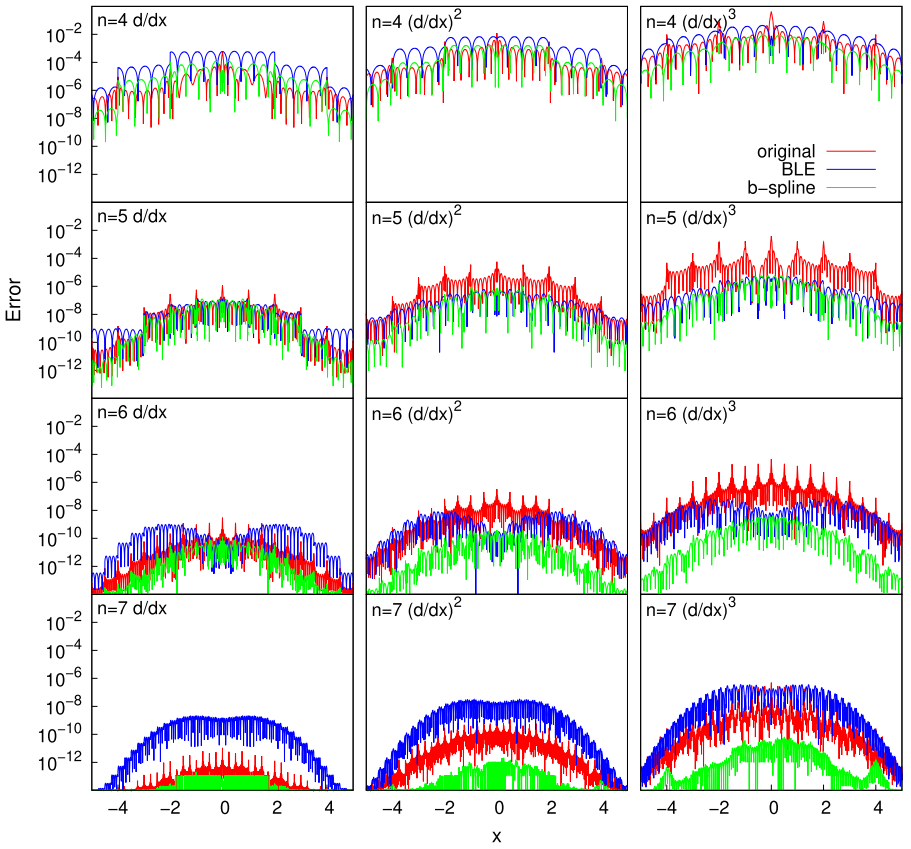

Fig. 3. For the original, b-spline and BLE constructions, the plot displays the absolute value of the error along the x-axis of the first, second and third derivatives w.r.t. x computed with repeated application of the first derivative operator applied in 3-dimensions to $f(x, y, z) = \left(\frac{\pi}{2}\right)^{(3/2)} e^{-(x^2+y^2+z^2)}$ projected into the k=10 scaling function basis in the cube $[-16, 16]^3$. Columns one, two and three correspond to the first, second and third derivatives, respectively. Rows one through four correspond to the test function being projected at levels 4 through 7, respectively.

grow only linearly with a near unit slope. Furthermore, examination of the right singular vector associated with the largest singular value of the original operator reveals a strong resemblance to a multiwavelet.

Figs. 6 and 7 demonstrate that we obtain the target order of accuracy and convergence. In Fig. 6, we demonstrate that for fixed $k = 7$ we obtain an error for all three b-spline derivatives that scales as $O\left(\omega^k\right)$ for small ω when applied to one of $\sin(\omega x)$ or $\cos(\omega x)$. In Fig. 7, we demonstrate that for fixed $\omega = 4.642$ we obtain for application to $\sin(\omega x)$ an error that asymptotically scales as $O\left(h^k\right)$ for all three b-spline derivatives (including the error arising from projection).

All three first derivative operators are examined in Figs. 8 and 9 with application to $\sin(\omega x)$ in the $k = 7$ basis. In Fig. 8, which should be compared with Fig. 6, we demonstrate that all three operators provide the expected scaling of the error with ω, and that the BLE and b-spline operators are more accurate than the original operators except at high ω or at low ω (where the accuracy of the BLE operator is constrained by the chosen accuracy of the quadrature rule). We cannot strictly speak of the frequency response or Fourier transform of the operators because they are applied on a finite, non-periodic domain, however, in Fig. 9 we examine the magnification factor (essentially the norm of the result) for each operator applied to $\sin(\omega x)$ as a function of ω. The large norm of the original operator is immediately apparent, as is the filtering properties of the other two operators, with the BLE construction filtering more strongly than the b-spline construction as already discussed above.

4.3. Kinetic energy in quantum mechanics

In non-relativistic quantum mechanics, the kinetic energy operator is essentially just the negative of the Laplacian. Thus, if the wave function describing the state is $f(x)$, the energy is given by

$$-\int f(x)^* \nabla^2 f(x) dx = \int (\nabla f(x))^\dagger . \nabla f(x) dx \tag{17}$$

with the equality holding for periodic or free-space boundary conditions. Similar integrals arise in other settings, for instance as the stiffness matrix in finite element analysis. The weak (second) form is especially interesting because its error is

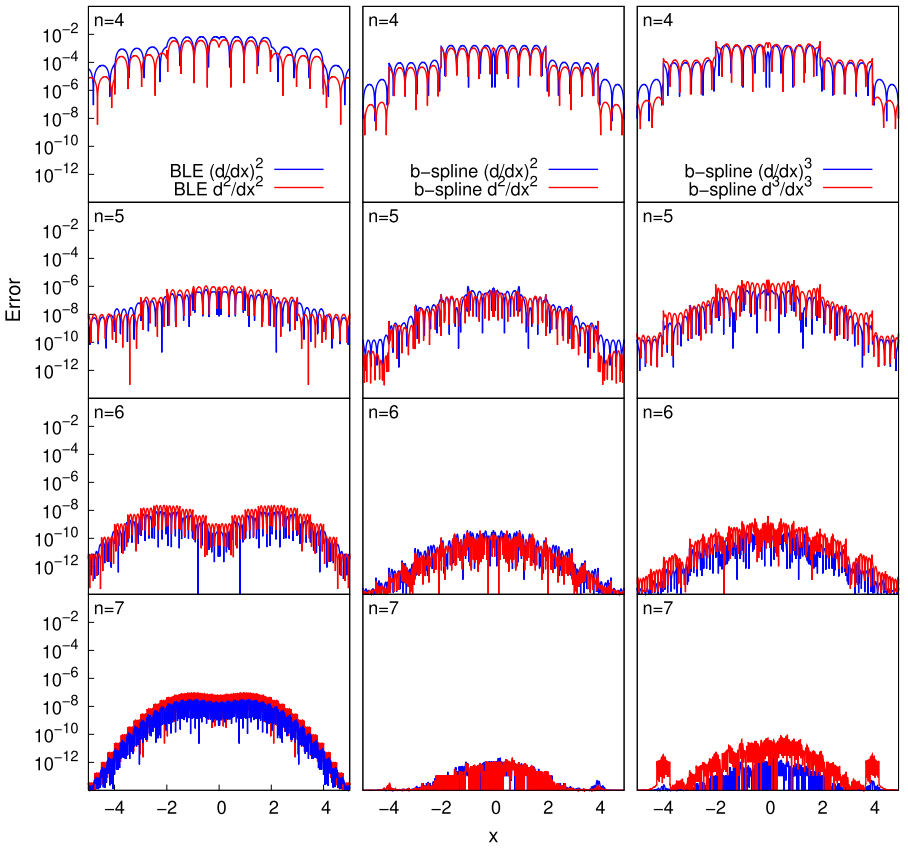

Fig. 4. For the second (BLE and b-spline) and third (b-spline) derivatives the plot contrasts the absolute value of the error obtained by either repeated application of the first derivative ($\left(\frac{d}{dx}\right)^p$ for $p = 2, 3$) or direct application of the higher-order derivative operator ($\frac{d^p}{dx^p}$) constructed as described in Section 3. The error is plotted along the x-axis and the target function is the same as in Fig. 3. The first column displays the BLE second derivative, and the second and third columns display the b-spline second and third derivatives, respectively. Rows one through four correspond to the test function being projected at levels 4 through 7, respectively.

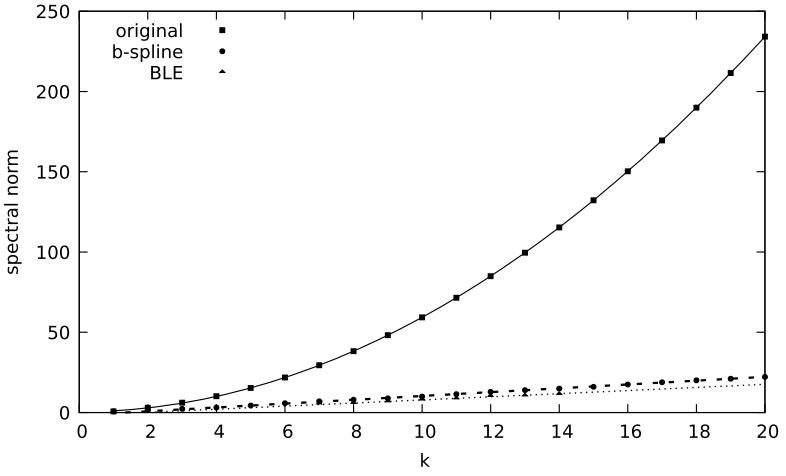

Fig. 5. For the original, b-spline and BLE 1st derivative operators the plot displays the spectral operator norms (maximum singular value) as a function of Legendre basis order (k). The points indicate the computed data and the lines are linear (b-spline and BLE) and quadratic (original) fits.

quadratic in the truncation threshold. This is the case for the 2-norm of any function in an orthonormal basis since the truncated component is orthogonal to that which is retained. However, only for the original derivative operator (a) does the equality numerically hold in (17) because only this operator is exactly antisymmetric, and (b) is truncation error the only error present since the other derivative operators introduce additional errors due to smoothing. Hence, the kinetic energy

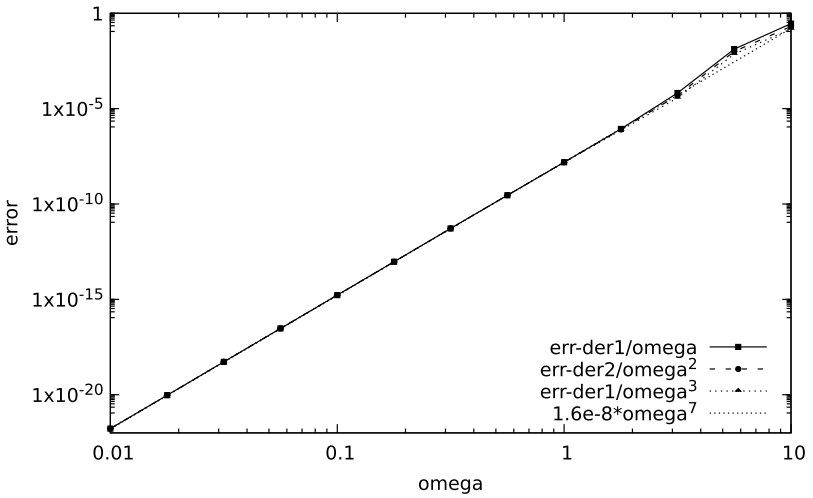

Fig. 6. For the b-spline operator construction the plot displays as a function of ω the 2-norm of the errors over $[0, 1]$ in the first and third derivatives of $\cos(\omega x)$ and the second derivative of $\sin(\omega x)$ with projection into the 3-box stencil over $[-1, 2]$ using the $k = 7$ Legendre basis. The derivatives are all of the form $\pm\omega^p \sin(\omega x)$ (for $p = 1, 2, 3$) and the plotted error is scaled by ω^{-p}. The trend line illustrates that the scaled error for all derivatives is $O(\omega^k)$, as expected.

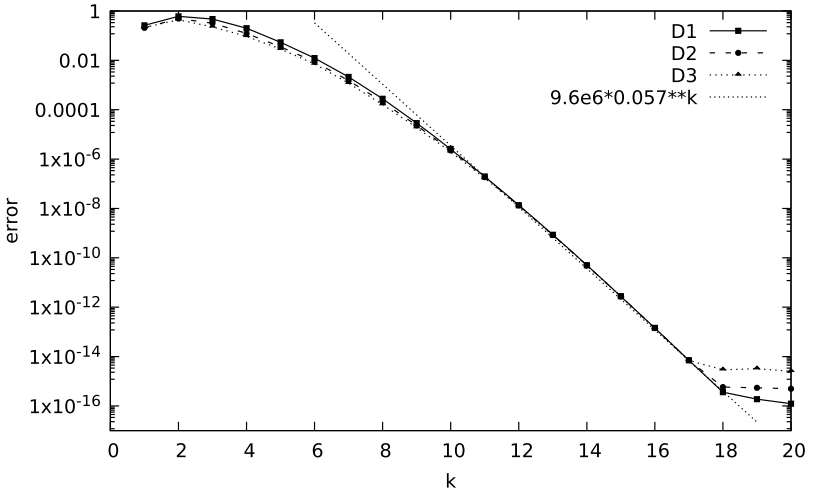

Fig. 7. 2-norm of the error over $[0, 1]$ in the first, second and third derivatives using the b-spline operators of $\sin(4.642x)$ with projection into the 3-box stencil over $[-1, 2]$ as a function of the order (k) of the Legendre basis. The trend line illustrates that the asymptotic error (arising from either projection or differentiation) is $O(h^k)$ as expected. The projection into the basis and computation of the derivative operators is done using 50 decimal digits in Maple, but the application of the operator and error computation is performed using standard double-precision arithmetic.

computed with the original operator enjoys quadratic convergence as we compute more accurately (in either a higher-order basis or at finer scales), whereas the smoothing implicit in the other derivative operators introduces an additional discrepancy that may converge less rapidly with the truncation threshold.

4.4. Consistency of integral and derivative operators

The new derivative operators provide a significant improvement (Table 1) in the consistency between the numerical and formal calculus as measured by the norm of the commutator $\left\| \left[\mu^2 - \nabla^2, \left(\mu^2 - \nabla^2\right)^{-1} \right] f(x) \right\|$. As noted in the introduction, with the original operator, nominally equivalent expressions may have very different error properties that can affect both accuracy and convergence. While rooted in the intrinsically different properties of the differential operator (that amplifies high frequencies) and the integral operator (that damps high frequencies), numerical computation exacerbates the issue by (1) injecting noise due to finite precision computation (i.e., after application of an operator projection into the discontinuous basis truncation to the requested precision), and (2) the nonphysical norm of the original derivative operator. The new operators do not completely eliminate this concern, but substantially reduce the need to over sample and for any order basis typically enhance the consistency by a factor of 10 or more.

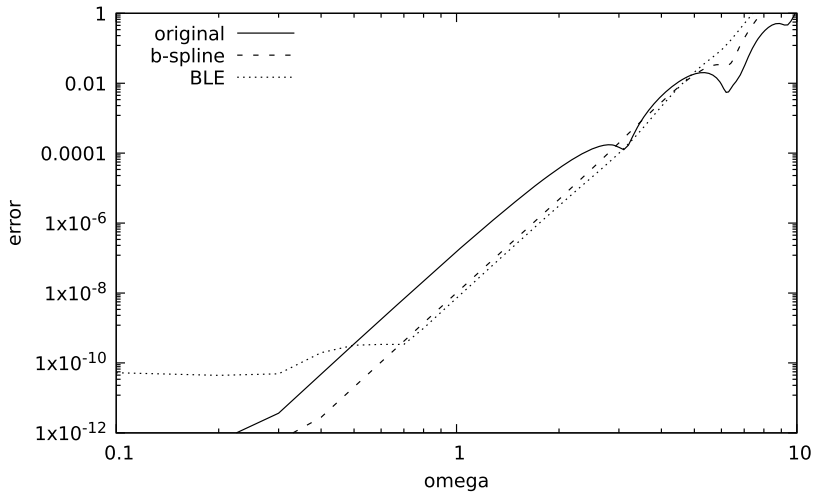

Fig. 8. For the original, b-spline and BLE first-derivative operators the plot displays as a function of ω the 2-norm of the error over $[0,1]$ in the first derivative of $\sin(\omega x)$ with projection into the 3-box stencil over $[-1,2]$ using the $k=7$ Legendre basis. The figure illustrates that (1) all constructions provide $O(\omega^{k+2})$ error for intermediate/small ω; (2) with the BLE construction being limited by the quadrature error for very small ω; and (3) for large ω the original construction is more accurate. The observed error is two orders smaller than in Fig. 6 above because the derivative here is $\omega\cos\omega x$, we have not scaled by ω^{-1}, and the Taylor expansion of cosine contains only even powers.

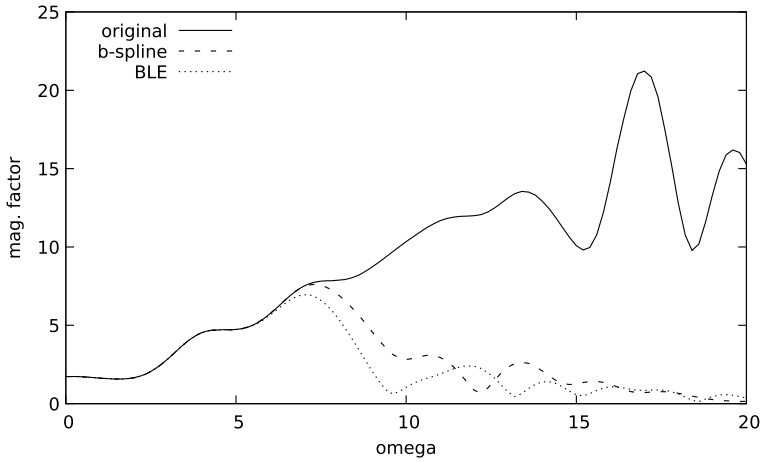

Fig. 9. For the original, b-spline and BLE derivative operators the plot displays as a function of ω the magnification factor ($\|Df\| / \|f\|$) for the first derivative of $sin(\omega x)$ with projection into the $k=7$ Legendre basis.

4.5. Structure of nuclear matter

One application of MADNESS lies in nuclear astrophysics. Using Density Functional Theory calculations in the Hartree-Fock approximation, MADNESS has been used to study nuclear pasta phases [34]. These are exotic shapes of nuclear matter that can exist in the crust of neutron stars and impact the stars' thermal and magnetic evolution as well as their oscillations and deformations ([10] and references therein). In Hartree-Fock, the nucleon single particle states $\psi_{i,q,s}$ with spin s, isospin q, mass m_q, and energy $E_{i,q}$ are subject to a mean-field potential U_q:

$$\left(-\hbar^2\Delta/(2m_q)+U_q\right)\psi_{i,q,s}=E_{i,q}\psi_{i,q,s}. \tag{18}$$

The potential can be described using Skyrme density functionals. For time-independent Hartree-Fock simulations of pasta phases with even numbers of neutrons and protons, it is given by:

$$\begin{aligned} U_q = {} & b_0\rho - b_0'\rho_q + b_1\tau - b_1'\tau_q - b_2\Delta\rho + b_2'\Delta\rho_q + b_3\frac{\alpha+2}{3}\rho^{\alpha+1} \\ & -b_3'\frac{2}{3}\rho^{\alpha}\rho_q - b_3'\frac{\alpha}{3}\rho^{\alpha-1}\left(\rho_n^2+\rho_p^2\right) - b_4\nabla\cdot\vec{J} - b_4'\nabla\cdot\vec{J}_q \\ & -\nabla\cdot\left(b_1\rho(\vec{r}) - b_1'\rho_q(\vec{r})\right)\nabla + \mathrm{i}\nabla\mathrm{b}_4\rho(\vec{\mathrm{r}}) + \mathrm{b}_4'\rho_{\mathrm{q}}(\vec{\mathrm{r}})\cdot\left(\vec{\sigma}\times\nabla\right). \end{aligned} \tag{19}$$

Table 1
For each of the derivative operators, this table examines the errors in the commutator of the differential operator $\hat{T} = \mu^2 - \nabla^2$ (with $\mu = 1$) and its inverse $\hat{T}^{-1} f(r) = \int \frac{e^{-\mu|r-r'|}}{|r-r'|} f(r') d^3r'$. Here, $f(r) = (\frac{10}{\pi})^{3/2} e^{-10r^2}$. The truncation threshold was 10^{-8}, and the 2-norm of $f(r)$ is approximately 1.41698.

k	Type	$\|\|\hat{T}\hat{T}^{-1}f - f\|\|_2$	$\|\|\hat{T}^{-1}\hat{T}f - f\|\|_2$	$\|\|[\hat{T},\hat{T}^{-1}]f\|\|_2$
7	original	1.09E-03	3.50E-07	1.09E-03
9	original	2.42E-04	2.00E-07	2.42E-04
11	original	2.86E-05	1.70E-07	2.86E-05
13	original	1.05E-05	1.00E-08	1.05E-05
15	original	1.57E-06	4.44E-09	1.56E-06
7	b-spline	7.38E-05	3.50E-07	7.38E-05
9	b-spline	1.17E-05	1.90E-07	1.16E-05
11	b-spline	1.26E-06	1.06E-06	1.64E-06
13	b-spline	3.10E-07	2.10E-07	3.70E-07
15	b-spline	1.30E-07	2.00E-08	1.30E-07
7	BLE	6.03E-05	3.60E-07	6.03E-05
9	BLE	6.40E-06	1.90E-07	6.36E-06
11	BLE	8.54E-06	6.50E-07	8.58E-06
13	BLE	9.20E-07	1.35E-06	1.62E-06
15	BLE	1.70E-07	9.00E-08	1.80E-07

The above term consists of a local potential, a potential accounting for the effective nucleon mass and a spin-orbit potential. For protons, Coulomb and Coulomb exchange potentials are also added. The neutron and proton number densities ρ_q, kinetic densities τ_q, and spin-orbit densities $\vec{J}_q$ are determined from the single particle states. The parameters b_j and b'_j are specific to a given Skyrme force. To study nuclear pasta phases in their ground state, the Bogoliubov-Hartree-Fock (BHF) equations are solved iteratively for several hundred to several thousand nucleons. At each iteration step, U_q is recalculated and used to update and orthonormalize the single particle states (for details, see [34]). Nuclear pasta phases are usually evolved over several thousand iteration steps until convergence is reached. At the same time, the Skyrme potential strongly depends on the derivatives of the single particle states as well as 1st and 2nd derivatives of functions that are determined from the states, e.g. ρ_q. Due to the non-linear, iterative nature of the simulations, small numerical noise in the derivatives can easily impact the single particle states and lead to unphysical results or even complete failure of the simulation. Unsatisfactory approaches to resolve this issue included computing to higher precision (which is expensive), damping or step restriction (which slows convergence), and Gaussian smoothing (which modifies the final result and must be removed before convergence). As shown in Fig. 10 for a BHF calculation on the O^{16} nucleus, the new derivative operators completely resolve this problem. With all derivative operators, the solution exhibits a small cusp or discontinuity in the derivative at iteration 28, but with the old operator the solution became unstable at iteration 29, despite already being very near convergence, and subsequently converged to a non-physical solution. However, both new operators converge uneventfully to the correct solution.

5. Conclusions

We have described a systematic approach for the construction of derivative operators by projecting to and from an intermediate basis with the desired properties and forming the derivative in that basis. For multiwavelet bases this construction advances beyond prior work [3] by (1) providing a systematic approach to forming second and higher derivatives; (2) controlling the amplification of high-frequency noise that inevitably arises in the use of these discontinuous, polynomial bases; and (3) enabling the generalization of the control of errors beyond that provided by the order of the polynomial basis and truncation threshold.

The construction was illustrated and its behavior analyzed for multiwavelet bases using both b-splines and bandlimited exponentials (BLE) as the intermediate basis. Both constructions showed high-order accuracy consistent with the order of the polynomial basis, linear increase in the spectral norm of the first derivative with the order of the polynomial basis, and strong suppression of high-frequency noise. However, the two operators also provide complementary properties that make each potentially valuable in different circumstances, as does the original operator:

- B-spline construction: the derivative operators are exact for polynomials (continuous over the input 3-box domain) up to the chosen order. This property makes it straightforward to construct operators that are consistent with the application's independent selection of polynomial order and truncation error, and hence to preserve the ability to use either h- or p-refinement to compute to any desired precision. In addition to high precision this also facilitates construction of low-order rules. The spectra of the operators are in general complex and are not consistent with those of the exact derivatives. Automatic construction of the b-spline operators is straightforward inside a tool such as Maple/Mathematica, facilitating application in other settings. So far only the central difference operator has been constructed.
- BLE construction: the underlying exponential basis results in derivative operators (with domain and range over the 3-box domain) having purely real/imaginary spectra consistent with those of the exact derivatives. Since the underlying

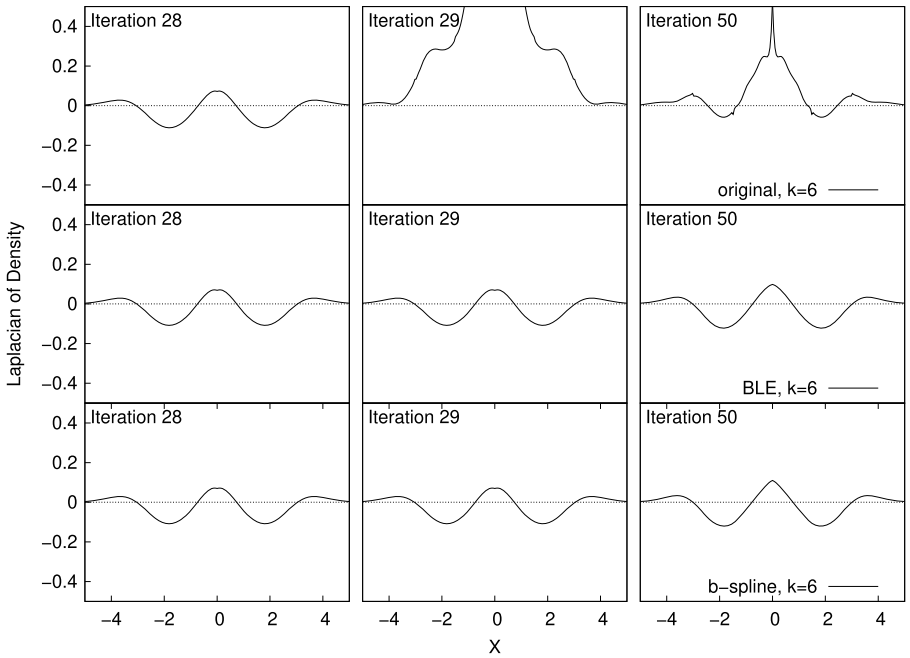

Fig. 10. For each derivative operator, the figure displays the Laplacian of the nuclear density at three iterations in the solution of the BHF equations for the O^{16} nucleus as described in Section 4.5. At iteration 28, the solution is nearly converged with a residual on the order of 10^{-5} for all three derivative operators, but visible is a small discontinuity in the first derivative for the computation. At iteration 29, the original operator yields a non-physical solution with a higher residual of 10^{-3}. By iteration 50 the solution with all three operators has converged but only the BLE and b-spline solutions agree with higher accuracy computations.

quadrature was constructed to be accurate to a specified threshold for all polynomials up to the chosen order, the error in the derivative operators is also similarly controlled — i.e., the expected order of approximation is obtained down to some finite error controlled by the accuracy of the quadrature. As a benefit of abandoning zero error at zero frequency, the BLE construction yields a slightly better error in the derivatives compared to that of the b-spline over a large range of frequencies until the stronger filtering of the BLE construction dominates the error. The construction of the BLE operators is much more complex than that of the b-splines and is presently not fully automated. Again, only the central difference operator has been constructed.

- Original construction: this is only feasible for the first derivative, and by construction the operator is antisymmetric and therefore has a purely imaginary spectrum. However, the spectral norm of the operator grows quadratically with the order of the polynomial, and the singular vectors corresponding to the largest singular values strongly resemble wavelets; hence, the original operator greatly amplifies the noise intrinsic to computation in the multiwavelet basis. The construction of the operator is straightforward with standard double-precision arithmetic, with central and forward/backward differences and also Dirichlet or Neumann boundary conditions [3].

We demonstrated the properties, advantages and limitations of the new derivative operators in several settings. In a nuclear quantum physics test case that involved the Laplacian of the density in the Hamiltonian, the new operators were both able to produce physically-correct solutions even when computing to low accuracy within MADNESS, whereas the original derivative operator failed except at higher accuracy which is computationally more expensive. The norm of the commutator of a differential operator and its numerical inverse as realized within MADNESS (convolution with separated representations of the corresponding Green's function) when applied to a test function was observed to be significantly smaller using the new derivative operators. Future work includes constructing integral operators that are optimally consistent with these new derivative operators.

Declaration of Competing Interest

The authors declare that they have no known competing financial interests or personal relationships that could have appeared to influence the work reported in this paper.

Acknowledgements

This work employed resources of the Institute for Advanced Computational Science at Stony Brook University including use of the Seawulf computer supported in part by the National Science Foundation under grant ACI-1531492. Anderson,

Harrison and Sundahl were supported in part by the NSF under grant ACI-1450344. Jensen was supported by the Norwegian Research Council through the CoE Hylleraas Centre for Quantum Molecular Sciences Grant No. 262695. Sagert was supported in part by DOE grants DE-FG02-87ER40365 and DE-SC0018083. Fann graciously acknowledges funding from the Scientific Discovery through Advanced Computing (SciDAC) project funded by the DOE Office of Advanced Scientific Computing Research (ASCR) and Nuclear Physics (NP); U.S. Department of Energy; the work was performed at the Oak Ridge National Laboratory, which is managed by is managed by UT-Battelle, LLC under Contract No. DE-AC05-00OR22725. The United States Government retains and the publisher, by accepting the article for publication, acknowledges that the United States Government retains a non-exclusive, paid-up, irrevocable, world-wide license to publish or reproduce the published form of this manuscript, or allow others to do so, for United States Government purposes.

Appendix A. Supplementary material

Supplementary material related to this article can be found online at https://doi.org/10.1016/j.jcpx.2019.100033.

References

[1] B. Alpert, A class of bases in L^2 for the sparse representation of integral operators, SIAM J. Math. Anal. 24 (1) (1993) 246–262.
[2] B. Alpert, G. Beylkin, R. Coifman, V. Rokhlin, Wavelet-like bases for the fast solution of second-kind integral equations, SIAM J. Sci. Comput. 14 (1) (1993) 159–184.
[3] B. Alpert, G. Beylkin, D. Gines, L. Vozovoi, Adaptive solution of partial differential equations in multiwavelet bases, J. Comput. Phys. 182 (1) (2002) 149–190.
[4] G. Beylkin, R. Coifman, V. Rokhlin, Fast wavelet transforms and numerical algorithms, I, Commun. Pure Appl. Math. 44 (2) (1991) 141–183; Yale Univ. Technical Report YALEU/DCS/RR-696, August 1989.
[5] G. Beylkin, L. Monzón, On generalized Gaussian quadratures for exponentials and their applications, Appl. Comput. Harmon. Anal. 12 (3) (2002) 332–373.
[6] G. Beylkin, L. Monzón, Efficient representation and accurate evaluation of oscillatory integrals and functions, Discrete Contin. Dyn. Syst. 36 (8) (2016) 4077–4100.
[7] G. Beylkin, K. Sandberg, Wave propagation using bases for bandlimited functions, Wave Motion 41 (3) (2005) 263–291.
[8] G. Beylkin, K. Sandberg, ODE solvers using bandlimited approximations, J. Comput. Phys. 265 (2014) 156–171, https://doi.org/10.1016/j.jcp.2014.02.001, see also arXiv:1208.3285.
[9] F. Bischoff, R. Harrison, E. Valeev, Computing many-body wave functions with guaranteed precision: the first-order moller-plesset wave function for the ground state of helium atom, J. Chem. Phys. 137 (2012).
[10] M.E. Caplan, C.J. Horowitz. Colloquium, Astromaterial science and nuclear pasta, Rev. Mod. Phys. 89 (4) (Oct. 2017) 041002.
[11] C. Chui, An Introduction to Wavelets, Academic Press, Boston, MA, 1992.
[12] I. Daubechies, Orthonormal bases of compactly supported wavelets, Commun. Pure Appl. Math. 41 (1988) 909–996.
[13] D.L. Donoho, N. Dyn, D. Levin, P.Y. Thomas, Smooth multiwavelet duals of alpert bases by moment-interpolating refinement, Appl. Comput. Harmon. Anal. 9 (2) (2000) 166–203.
[14] G. Fann, J. Pei, R.J. Harrison, J. Jia, M. Ou, W. Nazarewciz, N. Schunck, W.A. Shelton, Fast multiresolution methods for density functional theory in nuclear physics, J. Phys. Conf. Ser. 180 (2009) 012080.
[15] P. Federbush, A mass zero cluster expansion, Commun. Math. Phys. 81 (1981) 327–340.
[16] J. Fosso-Tande, R. Harrison, Implicit solvation models in a multiresolution multiwavelet basis, Chem. Phys. Lett. 561–562 (2013) 179–184.
[17] A. Haar, Zur Theorie der orthogonalen Funktionensysteme, Math. Ann. (1910) 331–371.
[18] R. Harrison, G. Fann, T. Yanai, G. Beylkin, Multiresolution quantum chemistry in multiwavelet bases, in: P.M.A. Sloot, et al. (Eds.), Computational Science-ICCS 2003, in: Lecture Notes in Computer Science, vol. 2660, Springer, 2003, pp. 103–110.
[19] R. Harrison, G. Fann, T. Yanai, Z. Gan, G. Beylkin, Multiresolution Quantum Chemistry: Basic Theory and Initial Applications, APPM preprint 516, Univ. of Colorado, December 2003.
[20] R. Harrison, G. Fann, T. Yanai, Z. Gan, G. Beylkin, Multiresolution quantum chemistry: basic theory and initial applications, J. Chem. Phys. 121 (23) (2004) 11587–11598.
[21] R.J. Harrison, G. Beylkin, F.A. Bischoff, J.A. Calvin, G.I. Fann, J. Fosso-Tande, D. Galindo, J. Hammond, R. Hartman-Baker, J.C. Hill, et al., Madness: a multiresolution, adaptive numerical environment for scientific simulation, SIAM J. Sci. Comput. 38 (5) (2016) S123–S142, see also arXiv preprint, arXiv:1507.01888.
[22] A. Harten, High resolution schemes for hyperbolic conservation laws, J. Comput. Phys. 49 (3) (1983) 357–393.
[23] A. Harten, High resolution schemes for hyperbolic conservation laws, J. Comput. Phys. 135 (2) (1997) 260–278.
[24] A. Harten, B. Engquist, S. Osher, S.R. Chakravarthy, Uniformly high order accurate essentially non-oscillatory schemes, iii, in: Upwind and High-Resolution Schemes, Springer, 1987, pp. 218–290.
[25] S.R. Jensen, T. Flå, D. Jonsson, R.S. Monstad, K. Ruud, L. Frediani, Magnetic properties with multiwavelets and dft: the complete basis set limit achieved, Phys. Chem. Chem. Phys. 18 (2016) 21145–21161.
[26] W.Y. Kong, V. Rokhlin, A new class of highly accurate differentiation schemes based on the prolate spheroidal wave functions, Appl. Comput. Harmon. Anal. 33 (2) (2012) 226–260, https://doi.org/10.1016/j.acha.2011.11.005.
[27] H.J. Landau, H.O. Pollak, Prolate spheroidal wave functions, Fourier analysis and uncertainty II, Bell Syst. Tech. J. 40 (1961) 65–84.
[28] H.J. Landau, H.O. Pollak, Prolate spheroidal wave functions, Fourier analysis and uncertainty III, Bell Syst. Tech. J. 41 (1962) 1295–1336.
[29] X.-D. Liu, S. Osher, T. Chan, Weighted essentially non-oscillatory schemes, J. Comput. Phys. 115 (1) (1994) 200–212.
[30] R.G. Parr, W. Yang, Density-Functional Theory of Atoms and Molecules, The International Series of monographs on Chemistry, vol. 16, Oxford Univ. Press, New York, 1989.
[31] J. Pei, M. Stoitsov, G. Fann, W. Nazarewicz, N. Schunck, F. Xu, Deformed coordinate-space Hartree-Fock-Bogoliubov approach to weakly bound nuclei and large deformations, Phys. Rev. C 78 (2008) 064306.
[32] J.C. Pei, G.I. Fann, R.J. Harrison, W. Nazarewicz, Y. Shi, S. Thornton, Adaptive multi-resolution 3d hartree-fock-bogoliubov solver for nuclear structure, Phys. Rev. C 90 (Aug. 2014) 024317.
[33] M. Reynolds, G. Beylkin, L. Monzón, On generalized Gaussian quadratures for bandlimited exponentials, Appl. Comput. Harmon. Anal. 34 (3) (2013) 352–365.

[34] I. Sagert, G.I. Fann, F.J. Fattoyev, S. Postnikov, C.J. Horowitz, Quantum simulations of nuclei and nuclear pasta with the multiresolution adaptive numerical environment for scientific simulations, Phys. Rev. C 93 (5) (May 2016) 055801.
[35] K. Sandberg, K. Wojciechowski, The EPS method: a new method for constructing pseudospectral derivative operators, J. Comput. Phys. 230 (15) (2011) 5836–5863.
[36] C.-W. Shu, S. Osher, Efficient implementation of essentially non-oscillatory shock-capturing schemes, J. Comput. Phys. 77 (2) (1988) 439–471.
[37] D. Slepian, Prolate spheroidal wave functions, Fourier analysis and uncertainty IV. Extensions, to many dimensions; generalized prolate spheroidal functions, Bell Syst. Tech. J. 43 (1964) 3009–3057.
[38] D. Slepian, Some asymptotic expansions for prolate spheroidal wave functions, J. Math. Phys. 44 (1965) 99–140.
[39] D. Slepian, Prolate spheroidal wave functions, Fourier analysis and uncertainty V. The discrete case, Bell Syst. Tech. J. 57 (1978) 1371–1430.
[40] D. Slepian, Some comments on Fourier analysis, uncertainty and modeling, SIAM Rev. 25 (3) (1983) 379–393.
[41] D. Slepian, H.O. Pollak, Prolate spheroidal wave functions, Fourier analysis and uncertainty I, Bell Syst. Tech. J. 40 (1961) 43–63.
[42] S. Takacs, T. Takacs, Approximation error estimates and inverse inequalities for b-splines of maximum smoothness, Math. Models Methods Appl. Sci. (2016) 1411–1445.
[43] N. Vence, R. Harrison, P. Krstic, Attosecond electron dynamics: a multiresolution approach, Phys. Rev. A 85 (3) (2012) 033403.
[44] H. Xiao, V. Rokhlin, N. Yarvin, Prolate spheroidal wavefunctions, quadrature and interpolation, Inverse Probl. 17 (4) (2001) 805–838.
[45] T. Yanai, G. Fann, Z. Gan, R. Harrison, G. Beylkin, Multiresolution quantum chemistry: analytic derivatives for Hartree-Fock and density functional theory, J. Chem. Phys. 121 (7) (2004) 2866–2876.
[46] T. Yanai, G. Fann, Z. Gan, R. Harrison, G. Beylkin, Multiresolution quantum chemistry: Hartree-Fock exchange, J. Chem. Phys. 121 (14) (2004) 6680–6688.
[47] T. Yanai, G.I. Fann, G. Beylkin, R.J. Harrison, Multiresolution quantum chemistry in multiwavelet bases: excited states from time-dependent hartree–fock and density functional theory via linear response, Phys. Chem. Chem. Phys. (2015).
[48] T. Yanai, R. Harrison, N. Handy, Multiresolution quantum chemistry in multiwavelet bases: time-dependent density functional theory with asymptotically corrected potentials in local density and generalized gradient approximations, Mol. Phys. 103 (2005).